CHAPTER – 5

Observation of Dielectric and Magnetic properties of $CaCu_3Ti_{4-X}Mn_XO_{12}$ (X= 0.0 and 0.1) ceramic synthesized through Semi-wet route

5.1 Introduction

The complex perovskite oxide has a general chemical formula $AA'_3B_4O_{12}$.In this complex perovskite system, A site is formed by alkali metals, alkaline earth metals, and lanthanides. B-site is formed by mainly transition metals. (Almeida et al. 2009),(Ahmadipour et al. 2018),(Adams et al. 2006)The size of A is larger than that of B. The metal ion which is occupied at the A site in the complex perovskite system, 12 fold coordinated unit squire planner. The metal ion B is occupied at the body-centered in the complex perovskite system in an octahedral arrangement. $ACu_3Ti_4O_{12}$ is a type of complex perovskite oxide widely known to belong to the Aurivillius family. The cation copper (d^9 configuration) present at the corner of the perovskite system, has a strong John-teller distortion.(Almeida et al. 2009),(Kumar et al. 2020b),(Ali et al. 2017),(Yadava et al. 2017) The tetravalent titanium (Ti^{+4}) occupied at the middle TiO_6octahedral. The complex perovskite system consists of two formula units. It is very different from the simple perovskite oxide ABO_3type. (Ahmadipour et al. 2018),(A. Molina-García and V. Rees 2016) ,(Zinatloo-Ajabshir et al. 2019),(De Almeida-Didry et al. 2014) The giant dielectric constant of $CaCu_3Ti_4O_{12}$ (CCTO) was first time discovered in 2000. The high dielectric constant of CCTO ceramic was recorded by weak temperature and frequency-dependent in the complex perovskite oxide. In the CCTO ceramic, there are several types of research available in theoretical and experimental. These works have been performed by the perspective of the supper capacitor application. Over the past several years, there are several applications have done by undoped and doped CCTO ceramic make them suitable for a large number of applications such as gas detectors, condensers, resonators, and memory devices. It is noted that besides these applications magnetic properties were also studied utilizing the high field of magnetization.(Supriya et al. 2017),(Jaiswar and Mandal 2017) There are

several studies of CCTO ceramic available such as Infrared spectroscopy, Raman studies, X-ray spectroscopy, X-ray photoelectron spectroscopy (XPS), Electrochemical impedance spectroscopy (EIS), High-Resolution Transmission Electron Microscopy (HR-TEM), Thermogravimetric analysis (TGA), Atomic Force Microscopy (AFM) by doping of pure and substituted CCTO ceramic. The antiferromagnetic transition (T_N) significantly changes by doping or substitution ion in the CCTO perovskite system. The CCTO ceramic has two sites for doping of ions which open up significant changes, making the compound with novel and improved physical properties. The doping or substitution of ion makes them suitable for future demands such as a variety of applications such as electronics and spintronics.

In this study, the magnetic properties were to be studied by doped and un-doped CCTO ceramic. The chemical formula of the ceramic was $CaCu_3T_{4-X}Mn\text{-}_XO_{12}$(X=0.0 and 0.1). The study was performed using M-H loop characteristics, DC magnetization FC and ZFC mode. When highly magnetic material Mn^{+4} ion doped into nonmagnetic titanium site, which is responsible for antiferromagnetic ordering. The dielectric properties were to be examined with the help of LCR meter.

5.2 Synthesis of materials

$CaCu_3Ti_4O_{12}$ (CCTO) and $CaCu3T_{3.9}Mn_{0.1}O_{12}$ (CCTMO) were successfully synthesized by the semi-wet process.For the production of CCTO and CCTMO ceramic $Ca(NO_3)_2{\cdot}4H_2O$ (99.2%, Merck, India), copper nitrate, $Cu(NO_3)_2{\cdot}3H_2O$ (99.8%, Merck, India),$Mn(CH_3COO)_2{\cdot}4H_2O$ (99% Merck, India), glycine (99%, Merck, India) and titanium oxide (TiO2 99% Merck, India) were taken in the two beakers in the stoichiometric ratio. Glycine was used as a chelating agent. Follow this solution mixture, at the magnetically stirred, the temperature was maintained 70 to 80°C for 12

to 15 h. The remaining quantity was dehydrated in a hot air oven. The powder of both ceramics was black. Then powder was ground. The samples were calcined at 600℃ for 12 h, follow these samples for Pelletization using Polyvinyl alcohol (2 wt. %). The PVA was burnt out at 500℃ for 2 h. The pellets were sintered at a 900℃ high-temperature furnace. The phase formation of both ceramics was to be examined by the X-ray diffraction pattern.

Characterization

The thermal behavior of CCTO and CCTMO ceramic was studied by Thermogravimetric analysis (TGA). The phase formation was to be analyzed by X-ray diffraction (XRD) pattern. The sample was characterized by Fourier Transform - Infrared spectroscopy (FT-IR). The microstructural studies were done through HR-SEM and HR-TEM. The stoichiometric ratio was to be confirmed by Energy Disperse X-ray (EDX). The magnetic properties and dielectric properties were to be studied.

5.3. Result and discussion

Thermogravimetric (TGA) analysis

Figure 5.1(a) and (b) display the thermal analysis of precursor powder of CCTO and CCTMO. It was recorded from room temperature to 1000℃ in the air with a heating rate of 10℃ per minute. The first weight loss occurred at 190℃ and 200℃ of CCTO and CCTMO, respectively. The second weight loss occurred at 190℃ to 500℃ for CCTO and 200℃ to 427℃ for CCTMO. (Kumar et al. 2020b) ,(Oliveira et al. 2017). The third weight loss occurred at 500 ℃ to 700℃ for CCTO and 427℃ to 710℃ for CCTMO. It is indicated from the TGA curve in this region the huge amount of weight loss occurred due to releasing a large amount of gases N_2, H_2O, and CO_2. It is pointed

from the curve that above 700°C, no furthered weight loss occurred, which indicates the phase formation of both ceramics.(Oliveira et al. 2017)

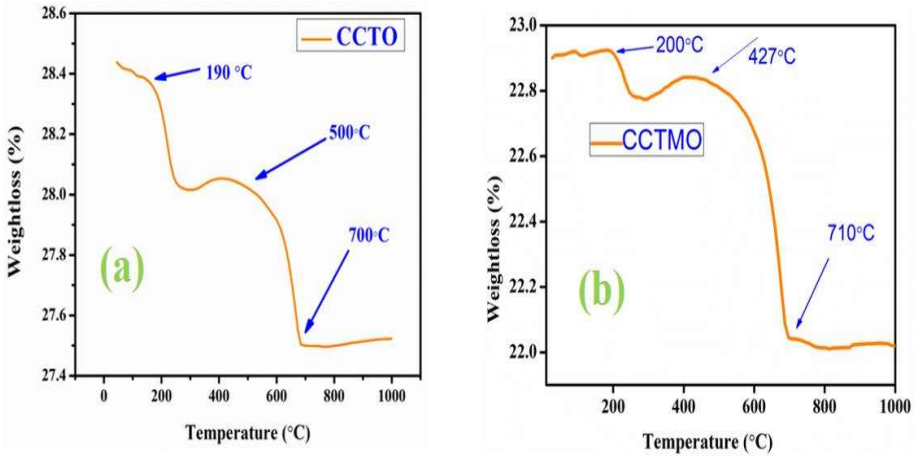

Figure 5.1. (a) and **(b)** display the TGA graph of CCTO and CCTMO respectively.

X-ray Diffraction (XRD) studies

Figure 5.2 (a) and (b) display the X-ray diffraction pattern (XRD) of CCTO and CCTMO ceramic sintered at 900°C for 12 h, respectively. All the peaks were indexed with the help of JCPDS No. 75-2188, single-phase formation takes place but only titanium oxide peak recorded in the CCTO ceramic. (Tripathy et al. 2016),(Kawrani et al. 2019)Based on the indexed d_{hkl} value of both the ceramic occupied body-centered cubic structure. The crystallite size of CCTO and CCTMO ceramic was to be calculated Scherer's equation

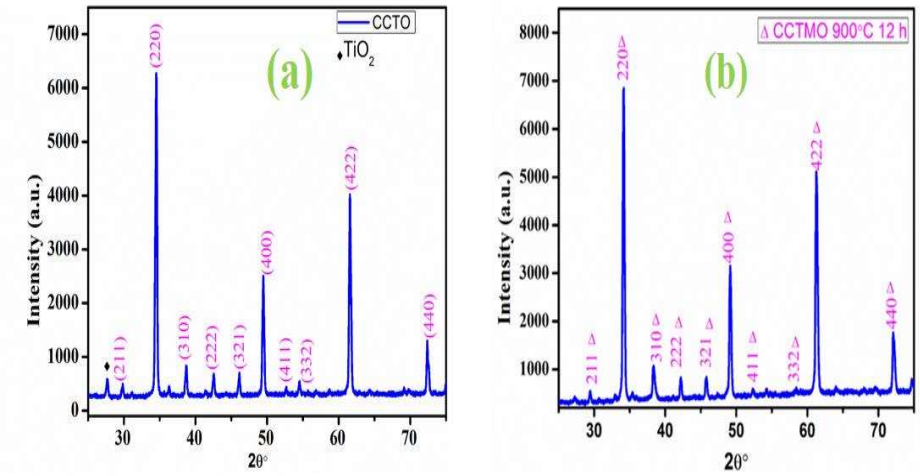

Figure 5.2. (a) and (b) display the XRD graph of CCTO and CCTMO respectively.

$$D = \frac{k\lambda}{\beta \cos \theta} \qquad \ldots\ldots\ldots\ldots \quad (1)$$

Where k is the crystal shape coefficient (k = 0.89), λ represents the wavelength (1.54 Å) of the X-ray. β represents the full-width half maxima (FWHM). From the above equation, θ is Bragg's diffraction angle. The crystallite size of CCTO and CCTMO was calculated to be 34.45 nm and 34.85 nm respectively.

Fourier Transform- Infrared spectroscopy (FT-IR) studies

The FT-IR spectra of CCTO and CCTMO ceramics are shown in Figure 5.3. The phase formation of both ceramics was confirmed by FT-IR. The bending mode of Cu-O may be responsible for the absorption peak found at 546 cm^{-1} (for CCTO) and 546 cm^{-1} (for CCTMO). The absorption peak was observed at 458 cm-1 (for CCTO) and 445 cm^{-1} (for CCTMO), and was thought to be caused by mixed Ti-O-Ti vibration mode. Kumar

et al. (Kumar et al., 2020b) The bending Mn-O bond may be responsible for the absorption peak reported at 405 cm^{-1} (for CCTO) and 398 cm^{-1} (for CCTMO). In the CCTO and CCTMO ceramics, mixed vibrations of CuO4 or MnO4 and TiO6 or MnO6 groups dominate, resulting in absorption bands in the 380–700 cm1 range. ((Oliveira et al., 2017)

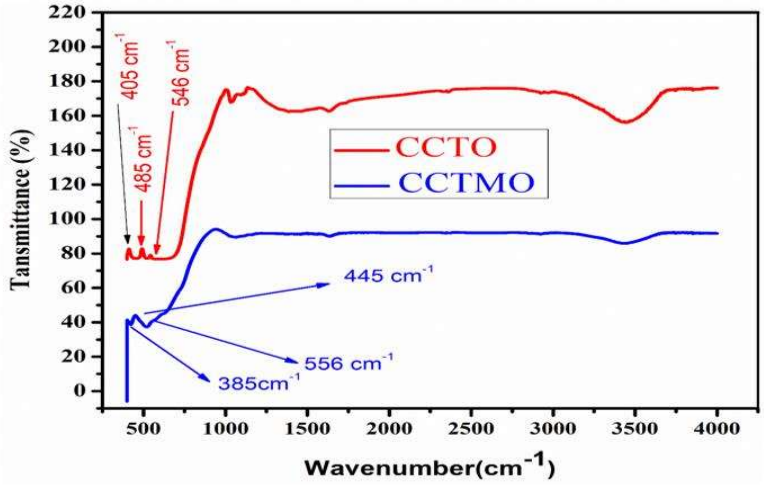

Figure 5.3. depict the FT-IR spectra of CCTO and CCTMO sintered 900°C for 12 h.

Raman studied

Figure 5.4 depicts the Raman spectrum of CCTMO ceramic sintered 900°C for 12 h. In the spectrum, the highest intensity peak was observed at 654 cm^{-1} and the lowest intensity peak was recorded at 428 cm^{-1}. The peak which is recorded at 428 cm^{-1} is may be due to the existence of CuO at the grain boundary. The peak observed at 589 cm^{-1} was to be associated with the A_1g symmetry octahedral MnO_6 rotation. From observing peaks it was to be confirmed that CuO in the grain boundary of CCTMO ceramic .(Chen et al. 2008),(Kolev et al. 2002)

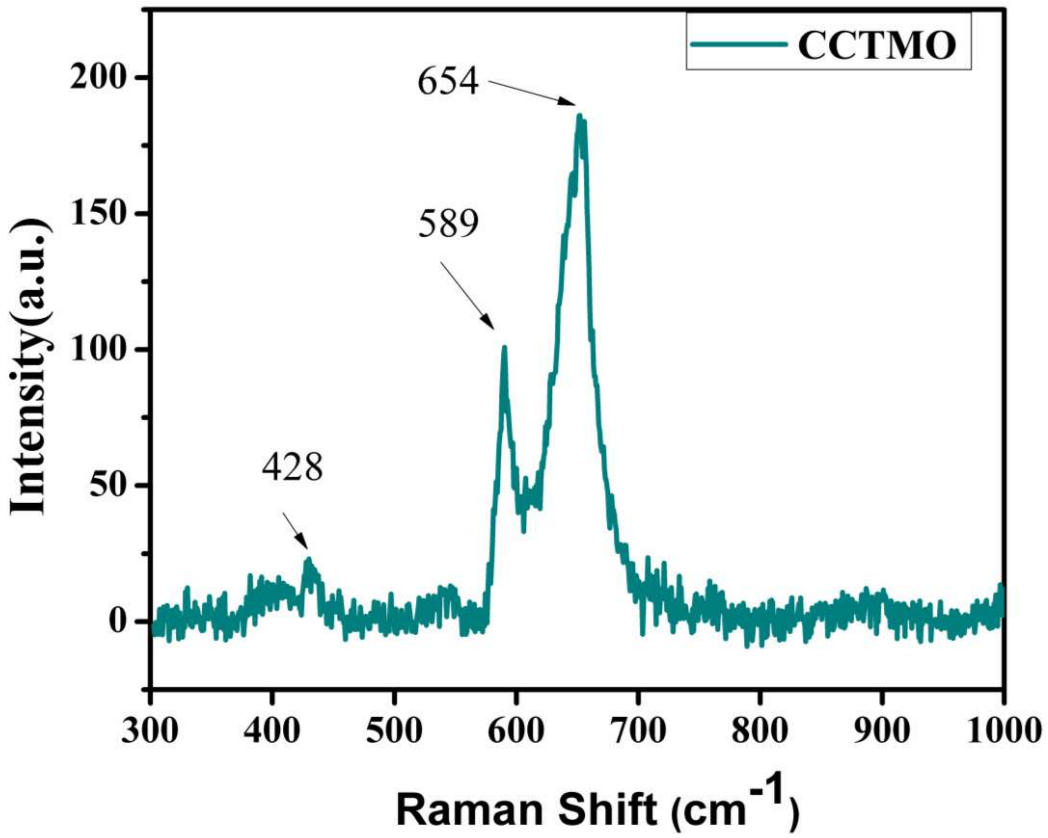

Figure 5.4. shows the Raman spectra of CCTMO ceramic .

5.3.1. Microstructural Studies

High Resolution- Scanning Electron Microscopic studies (HR-SEM)

Figure5.5(a) and (b) display the microstructural image of CCTO and CCTMO ceramic sintered 900℃ for 12 h.The grains and grain boundaries in both ceramics are well separated.The grains are polygonal shape however, some grains are observed spherical shape of both CCTO and CCTMO ceramic.It is observed that the grain of CCTO ceramic in a specific style to each other as compared to CCTMO ceramic. There is no unwanted distortion that occurs in both ceramics.The grain size of CCTO and CCTMO

ceramic were to be observed 439.64 nm and 409.10 nm respectively.

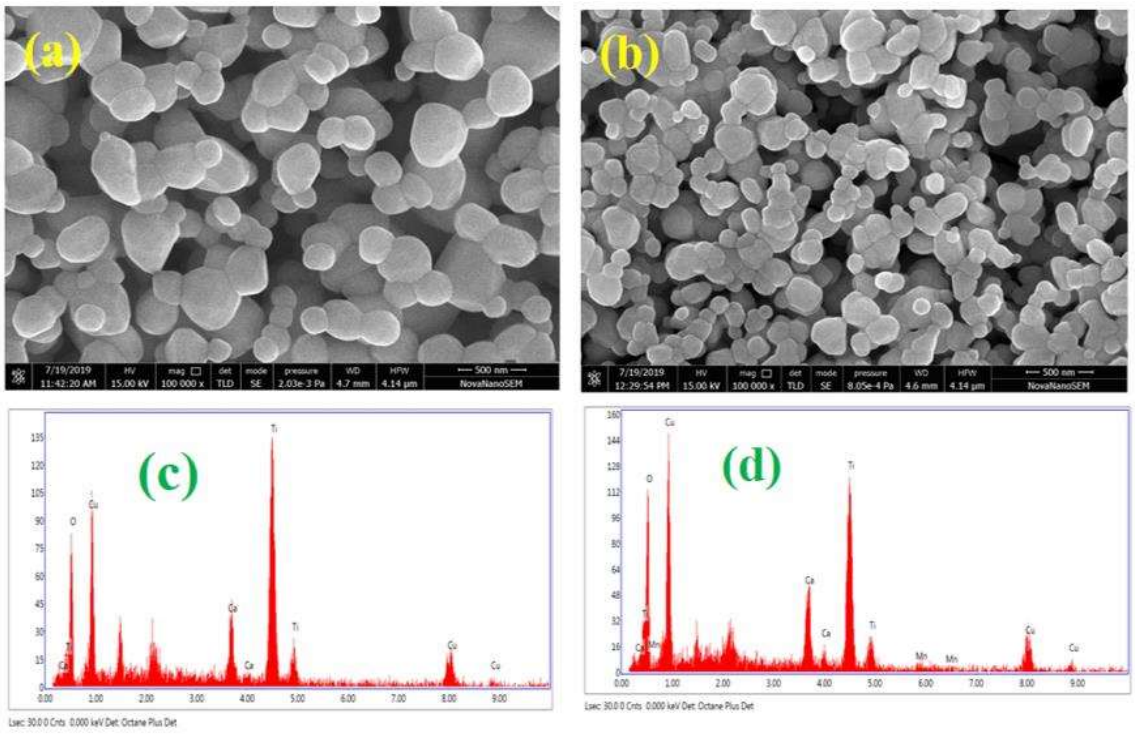

Figure 5.5. display **(a)** and **(b)** the HR-SEM of CCTO and CCTMO ceramic sintered 900℃ respectively. **(c)** and **(d)** EDX spectrum of CCTO and CCTMO ceramic respectively.

High Resolution -Transmission Electron Microscopic studies (HR-TEM)

Figure 5.6. (a) depicts the bright-field TEM image of CCTMO ceramic. The bright-field image of CCTO ceramic was published in our earlier research paper.(Kumar et al. 2020a) The average particle size of CCTMO was to be observed at 214 nm. The particle images looking at cubical structure. Figure 5b displays the SEAD pattern Of CCTMO

ceramic. This data is also verified by the XRD data. (Liu et al. 2011)

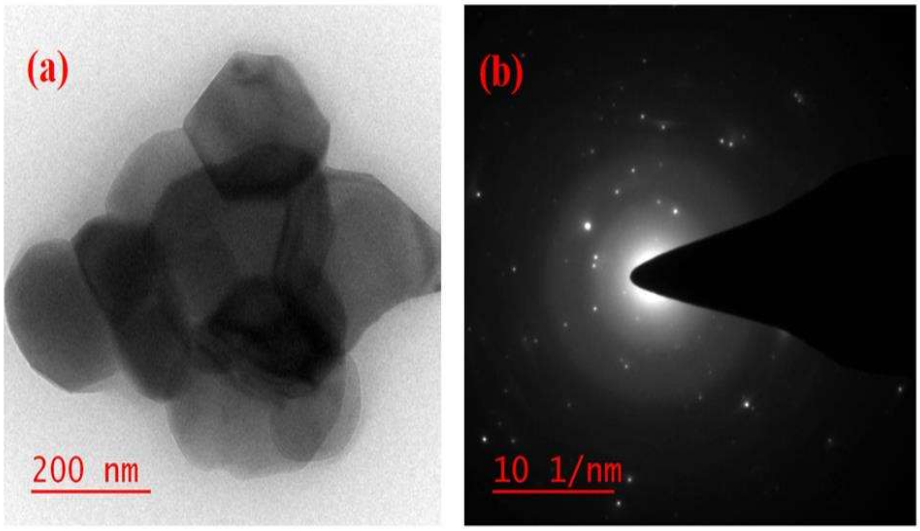

Figure 5.6. displays **(a)** The HR-SEM image of CCTMO ceramic (cubical structure), **(b)** the SEAD pattern of CCTMO ceramic.

5.3.2. Magnetic Properties studies

Figure 5.7 (a) illustrates the magnetization (emu/g) of CCTO and CCTMO ceramics versus the magnetic field. This was observed in the range of 60 kOe at 300 K (main panel) to 5 K. (inset figure). The ferromagnetic properties of CCTO and CCTMO compound perovskite are found to that CCTO exhibit weak as compared to CCTMO. At 300 K, CCTO and CCTMO ceramics have zero coercivity. The plotted graph clearly shows that the saturation of the magnetization curve does not occur even at 60 kOe field, indicating a non-colinear spin arrangement. (Slimani et al. 2018)Copper exists in (S = 1/2 spins) in both ceramics, it is noted. Both ceramics exhibit paramagnetic properties. The plotted curve shows that when manganese (Mn) was doped into the CCTO ceramic, the magnetic character increased. The paramagnetic nature of CCTMO is stronger than that of CCTO ceramic. Coercivity and remanence are both zero in both ceramics. The curve from the plotted of CCTMO ceramic free of anisotropy ion (Mn^{+2})

shows that magnetic anisotropy non-collinear spin arrangement occurs, as shown by the above reasoning. (Berry et al. 2000)

The temperature fluctuation of magnetization in the ZFC and FC states is depicted in Figure 5.7(b). The external magnetic field of 10 mT was used to characterized both the ceramics (CCTO and CCTMO). The zero-field cooled (ZFC) and field-cooled (FC) magnetization curves display reversible behavior, as seen in the plotted graph. The Neel temperature (T_N) transition was recorded in CCTO and CCTMO ceramic at 25 K and 23.1 K . Kim at al was the first time observed the transition region. It is pointed out that when Manganese doped into the CCTO ceramic at the titanium site it was strongly affected on antiferromagnetic transition (T_N). (Chen et al. 2016),(Yadava et al. 2017)

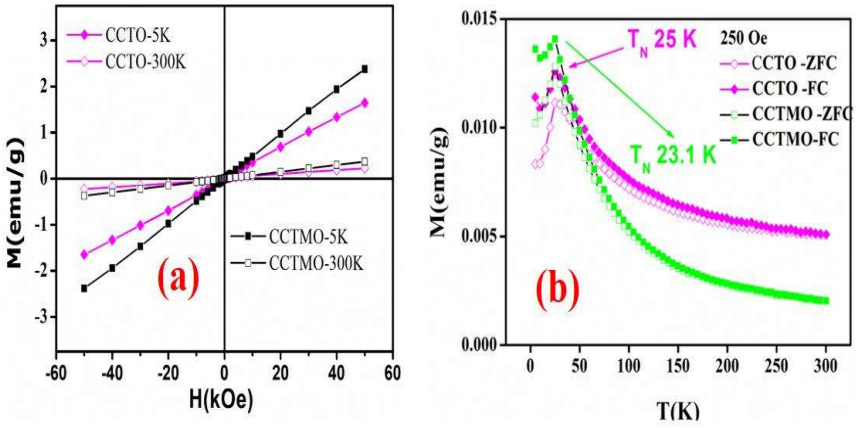

Figure 5.7. display **(a)** the magnetization versus magnetic field **(b)** magnetization versus temperature of CCTO and CCTMO.

5.3.3. Dielectric studied

It is observed from Figure 5.8 (a) and (C) frequency and temperature dependence dielectric constant of CCTMO ceramic. The dielectric constant was to be recorded at few selected temperatures and frequencies 310 K, 350 K, 390 K, 430 K and 100 Hz, 1 KHz, 10 KHz, 100 KHz respectively. It was to be examined that the dielectric

constant of CCTMO ceramic 500 against frequency (Hz) and 150 against temperature (K). It is observed from figure 5.7 (a) that the dielectric decrease rapidly at higher frequency this is may be due to positive and negative charges separation not take place. It is observed from figure 5.7 (C) the dielectric constant is independent of temperature. Ferroelectric relaxation observed in the CCTMO ceramic. (Rani et al. 2018),(Pandey and Mandal 2019)It is observed from the figure when Manganese doped in the $CaCu_3Ti_4O_{12}$ (CCTO) ceramic largely decreases the dielectric constant. This was due to grain and grain boundaries slightly conducting in nature. The dielectric constant of CCTO ceramic was already reported in our earlier research paper.(Kumar et al. 2020a)

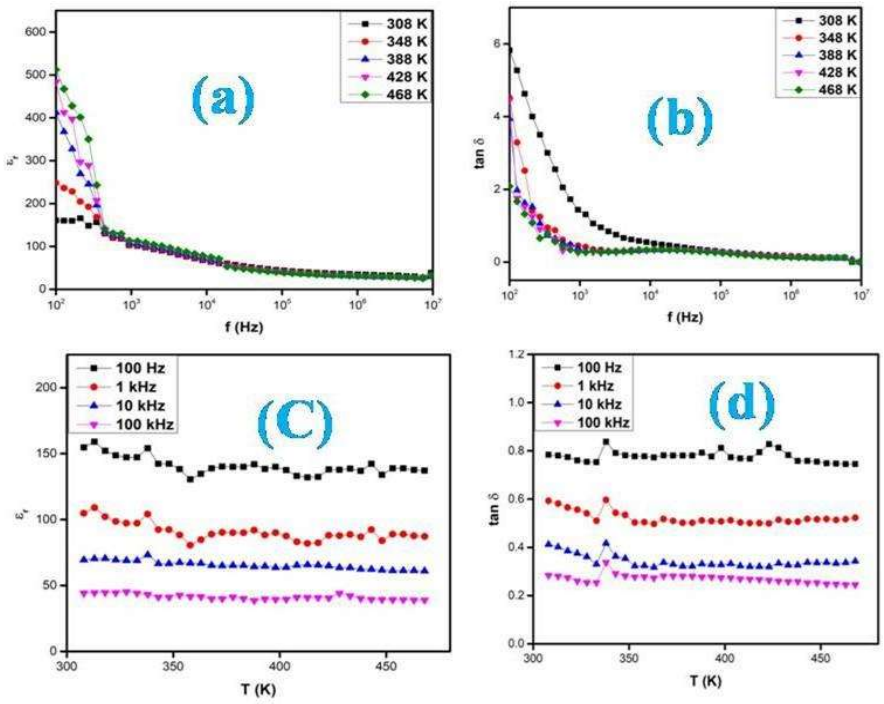

Figure 5.8. (a) and (c) show the dielectric constant versus frequency and temperature respectively, figure (b) and (d) depicts the tangent loss versus frequency and temperature respectively.

It is observed from figure 5.8 (b) and (d) temperature and frequency-dependent tangent loss of CCTMO ceramic. It was to be recorded at few selected temperatures and frequency 310 K , 350 K,390 K ,430 K and 100 Hz, 1 kHz,10KHz 100KHz . Figure 5.8 (b) depicts the tangent loss of CCTMO ceramic against frequency. From the figure, it is clear that tangent loss decreases with increasing frequency. From figure 5.8 (d) the tangent loss of CCTMO ceramic was to be observed approximately 0.8 at 100 Hz frequency.

5.4. Conclusions

The CCTO and CCTMO ceramic were to be successfully synthesized through a semi-wet route. The thermal behavior was to be studied by TGA, the first weight loss was to be observed at 190℃ and 200℃ of CCTO and CCTMO, respectively. At reaching above temperature 700 ℃ and 710 ℃ for CCTO and CCTMO no further weight loss happened which indicates the phase formation of both ceramic respectively. The phase formation was to be confirmed by XRD. Raman spectra confirmed that CuO was exist at the grain boundary of the CCTMO ceramic. The crystallite size was to be observed 34.45 nm and 34.85 nm CCTO and CCTMO, respectively. From the FTIR spectra, it is observed that there are absorption bands in the region 380 –700 cm^{-1} arising from the mixed vibrations of CuO_4 or MnO_4 and TiO_6 or MnO_6 groups dominant in the CCTO and CCTMO ceramic. The grain size of CCTO and CCTMO ceramic were to be observed 439.64 nm and 409.10 nm respectively. The particle size of CCTMO has been calculated 214 nm which is looking in cubical structure. The M (H) curve indicates that the materials are low anisotropy magnetic materials with a non-collinear spin structure. It was to be observed from the M (T) curve that the Neel transition temperature to the

recorded at 25 K for the CCTO and 23.1 K for the CCTMO ceramic. The maximum dielectric constant of CCTMO ceramic was found to 5×10^2 at 308 K temperature and the minimum tangent loss was to be recorded at 0.8 at 100 Hz frequency.

References

Adams, T.B., Sinclair, D.C., West, A.R., 2006. Influence of Processing Conditions on the Electrical Properties of CaCu3Ti4O12 Ceramics. *Journal of the American Ceramic Society* **89**, 3129–3135. https://doi.org/10.1111/j.1551-2916.2006.01184.x

Ahmadipour, M., Cheah, W.K., Ain, M.F., Rao, K.V., Ahmad, Z.A., 2018. Effects of deposition temperatures and substrates on microstructure and optical properties of sputtered CCTO thin film. *Materials Letters* **210**, 4–7. https://doi.org/10.1016/j.matlet.2017.08.121

Ali, K., Bahadur, A., Jabbar, A., Iqbal, S., Ahmad, I., Bashir, M.I., 2017. Synthesis, structural, dielectric and magnetic properties of CuFe2O4/MnO2 nanocomposites. *Journal of Magnetism and Magnetic Materials* **434**, 30–36. https://doi.org/10.1016/j.jmmm.2016.12.009

Almeida, A.F.L., Fechine, P.B.A., Graça, M.P.F., Valente, M.A., Sombra, A.S.B., 2009. Structural and electrical study of CaCu3Ti4O12 (CCTO) obtained in a new ceramic procedure. *J Mater Sci: Mater Electron* **20**, 163–170. https://doi.org/10.1007/s10854-008-9675-4

A. Molina-García, M., V. Rees, N., 2016. Effect of catalyst carbon supports on the oxygen reduction reaction in alkaline media: a comparative study. *RSC Advances* **6**, 94669–94681. https://doi.org/10.1039/C6RA18894J

Berry, F.J., Greaves, C., Helgason, Ö., McManus, J., Palmer, H.M., Williams, R.T., 2000. Structural and Magnetic Properties of Sn-, Ti-, and Mg-Substituted α-Fe2O3: A Study by Neutron Diffraction and Mössbauer Spectroscopy. *Journal of Solid State Chemistry* **151**, 157–162. https://doi.org/10.1006/jssc.1999.8605

Chen, J., Dai, H., Chen, Z., Li, T., Liu, D., 2016. Effect of CaCu3Ti4O12 modification on the structural, electrical and magnetic properties of BiFeO3 ceramics. *Ferroelectrics* **504**, 123–129. https://doi.org/10.1080/00150193.2016.1240003

Chen, K., Wu, Y., Liao, J., Liao, J., Zhu, J., 2008. RAMAN AND DIELECTRIC SPECTRA OF CaCu3Ti3.9O12 CERAMICS. *Integrated Ferroelectrics* **97**, 143–150. https://doi.org/10.1080/10584580802089023

De Almeida-Didry, S., Autret, C., Lucas, A., Honstettre, C., Pacreau, F., Gervais, F., 2014. Leading role of grain boundaries in colossal permittivity of doped and undoped CCTO. *Journal of the European Ceramic Society* **34**, 3649–3654. https://doi.org/10.1016/j.jeurceramsoc.2014.06.009

Jaiswar, S., Mandal, K.D., 2017. Evidence of Enhanced Oxygen Vacancy Defects Inducing Ferromagnetism in Multiferroic CaMn7O12 Manganite with Sintering Time. *J. Phys. Chem. C* **121**, 19586–19601. https://doi.org/10.1021/acs.jpcc.7b05415

Kawrani, S., Boulos, M., Cornu, D., Bechelany, M., 2019. From Synthesis to Applications: Copper Calcium Titanate (CCTO) and its Magnetic and Photocatalytic Properties. *ChemistryOpen* **8**, 922–950. https://doi.org/10.1002/open.201900133

Kolev, N., Bontchev, R.P., Jacobson, A.J., Popov, V.N., Hadjiev, V.G., Litvinchuk, A.P., Iliev, M.N., 2002. Raman spectroscopy of ${\mathrm{CaCu}}_{3}{\mathrm{Ti}}_{4}{\mathrm{O}}_{12}$. *Phys. Rev. B* **66**, 132102. https://doi.org/10.1103/PhysRevB.66.132102

Kumar, V., Kumar, A., Verma, M.K., Singh, S., Pandey, S., Rai, V.S., Prajapati, D., Das, T., Singh, N.B., Mandal, K.D., 2020a. Investigation of dielectric and electrochemical behavior of CaCu3−xMnxTi4O12 (x = 0, 1) ceramic synthesized through semi-wet route. *Materials Chemistry and Physics* **245**, 122804. https://doi.org/10.1016/j.matchemphys.2020.122804

Kumar, V., Kumar, A., Verma, M.K., Singh, S., Pandey, S., Singh, L., Singh, N.B., Mandal, K.D., 2020b. Observation of unusual Griffith's phase behavior in quadruple perovskite oxide CaCu3Mn4O12 (CCMO) synthesized through chemical route. *Arabian Journal of Chemistry* **13**, 4895–4903. https://doi.org/10.1016/j.arabjc.2020.01.003

Liu, Q.X., Tang, X.G., Jiang, Y.P., Dong, F.L., 2011. The Dielectric Characteristics of Sr and Mg Doped CCTO Ceramics. *Materials Science Forum* **687**, 416–421. https://doi.org/10.4028/www.scientific.net/MSF.687.416

Oliveira, G.F. de, Andrade, R.C. de, Trindade, M.A.G., Andrade, H.M.C., Carvalho, C.T. de, 2017. Thermogravimetric and spectroscopic study (TG–DTA/FT–IR) of activated carbon from the renewable biomass source babassu. *Quím. Nova* **40**, 284–292. https://doi.org/10.21577/0100-4042.20160191

Pandey, S., Mandal, K.D., 2019. Investigation of microstructure, ferroelectric and dielectric behavior of CaCu3Ti(4−x)MnxO12 perovskites synthesized through semi-wet route. *SN Appl. Sci.* **1**, 1738. https://doi.org/10.1007/s42452-019-1647-1

Rani, S., Ahlawat, N., Sangwan, K.M., Rani, S., Punia, R., Malik, J., 2018. Structural investigation and giant dielectric response of CaCu3Ti4O12 ceramic by Nd/Zr co-doping for energy storage applications. *J Mater Sci: Mater Electron* **29**, 10825–10833. https://doi.org/10.1007/s10854-018-9150-9

Slimani, Y., Baykal, A., Amir, Md., Tashkandi, N., Güngüneş, H., Guner, S., El Sayed, H.S., Aldakheel, F., Saleh, T.A., Manikandan, A., 2018. Substitution effect of Cr3+ on hyperfine interactions, magnetic and optical properties of Sr-hexaferrites. *Ceramics International* **44**, 15995–16004. https://doi.org/10.1016/j.ceramint.2018.06.033

Supriya, D.M., Rajani, M.R., Phani, A.R., Naveen, C.V.S., Ravishankar, R., 2017. Synthesis of CCTO and Doped CCTO Nanopowders and its Applications in the Field of Electronics. *Materials Today: Proceedings*, INTERNATIONAL CONFERENCE ON NANOTECHNOLOGY (ICNANO-2016), APRIL 21-23, 2016, Bangalore, Karnataka **4**, 12021–12025. https://doi.org/10.1016/j.matpr.2017.09.125

Tripathy, N., Das, K.C., Ghosh, S.P., Bose, G., Kar, J.P., 2016. Fabrication of high-k dielectric Calcium Copper Titanate (CCTO) target by solid state route. *IOP Conf. Ser.: Mater. Sci. Eng.* **115**, 012022. https://doi.org/10.1088/1757-899X/115/1/012022

Yadava, S.S., Khare, A., Gautam, P., Kumar, A., Mandal, K.D., 2017. Dielectric, ferroelectric and magnetic study of iron doped hexagonal Ba4YMn3O11.5−δ

(BYMO) and its dependence on temperature as well as frequency. *New J. Chem.* **41**, 4611–4617. https://doi.org/10.1039/C6NJ04071C

Zinatloo-Ajabshir, S., Salehi, Z., Salavati-Niasari, M., 2019. Synthesis of dysprosium cerate nanostructures using Phoenix dactylifera extract as novel green fuel and investigation of their electrochemical hydrogen storage and Coulombic efficiency. *Journal of Cleaner Production* **215**, 480–487. https://doi.org/10.1016/j.jclepro.2019.01.026